Type of paper: letter (Journal of Geotechnical and Geoenvironmental Engineering – Technical Note)
Date text written: January 2020
Date text revised: 06/2020
Number of words in main text and tables = 2913
Number of figures = 6
Number of tables = 1

---

# Impact of three-dimensional sphericity and roundness on coordination number

Author 1
Wenbin Fei, PhD student, ME, BE
Department of Infrastructure Engineering, The University of Melbourne, Parkville, Australia
ORCID: 0000-0002-9275-8403

Author 2
Guillermo A. Narsilio ✉, PhD, MSc (Math), MSc (CE), CEng
Department of Infrastructure Engineering, The University of Melbourne, Parkville, Australia
ORCID: 0000-0003-1219-5661

✉ Full contact details of corresponding author
Guillermo A. Narsilio, Associate Professor in Geotechnical Engineering
Engineering Block B 208, Department of Infrastructure Engineering, The University of Melbourne, Parkville, VIC 3010, Australia
Email: narsilio@unimelb.edu.au, Phone: +61 (3) 8344 4659, Fax: +61 (3) 8344 4616

**ABSTRACT**

Coordination number (CN) is a fundamental micro-scale variable in soils affecting the macroscale parameters of the material such as porosity, stiffness under loading and stability under hydraulic gradients. However, most studies on CN have focused on sphere or ellipsoid packings using discrete element method (DEM). By means of computed tomography (CT) and image processing techniques, this work rigorously computes the three-dimensional sphericity and roundness of each grain in five sands and investigates the impact of particle shape on CN. The results show that the average coordination number ($CN_{ave}$) of *different* sands and the CN of grains *within a given* sand may be impacted differently by particle shape. For a given equivalent diameter of a given sand, more irregular grain packings show a subtle higher CN, this change in CN increases with increasing grain size. However, air-pluviated irregular particle packings with poor gradation may exhibit lower average $CN_{ave}$ because of particle orientational alignment, particle interlocking and surface roughness.

**KEYWORDS:** particle-scale behaviour; fabric/structure of soils; sands

# INTRODUCTION

Coordination number (CN) quantifies how many neighbouring particles surround a given particle in a granular material. The *average* coordination number ($CN_{ave}$) of a soil affects the macroscale behaviour and characterising parameters of the assembly. Shear-wave velocity in sandstones can be estimated using $CN_{ave}$ (Wang et al. 2019). The internal stability of a material under compaction or seepage force can also be indicated by $CN_{ave}$. Triaxial compression tests revealed that higher shear stiffness was attributed to higher $CN_{ave}$ in sands (Fonseca et al. 2013). Hence, materials with high $CN_{ave}$ can be used to minimise particle breakage in pavements (Minh and Cheng 2013). The stability of an embankment filter may decrease as $CN_{ave}$ reduces monotonically in both sphere packings (Shire and O'Sullivan 2013) and real sands (Fonseca et al. 2014). As $CN_{ave}$ shows great importance, a study of how it is affected by particle geometry (e.g. shape, gradation, friction, cohesiveness) is necessary because these geometrical attributes may guide the material selection in engineering applications.

$CN_{ave}$ generally increases with the particle size in non-uniform sphere packings (Minh and Cheng 2013). A better gradation can also increase the $CN_{ave}$ in sphere packings (Minh and Cheng 2013). In the discrete element method (DEM) study of packings of super-ellipsoids that can be represented by Equation 1 (i.e., oblate and prolate spheroids), the correlation between $CN_{ave}$ and aspect ratio (aspect ratio is '*c*' in Equation 1 after setting '*a*' = '*b*' = 1) shows an 'M' shape (Delaney and Cleary 2010; Donev et al. 2004; Gan et al. 2017; Zhou et al. 2011) with the lowest $CN_{ave}$ found at an aspect ratio of 1 (a sphere packing always has the lowest $CN_{ave}$). Additionally, the $CN_{ave}$ reduces when ` shape parameter '*m*' changes from 3 to 5 (in Equation 1, increasing '*m*' from 2 make a sphere more cubic-like in shape) (Delaney and Cleary 2010) because of high particle orientational alignment:

$$\left(\frac{x}{a}\right)^m + \left(\frac{y}{b}\right)^m + \left(\frac{z}{c}\right)^m = 1 \quad (1)$$

where *m* is a shape parameter. *a*, *b* and *c* are principal axis lengths.

Similar results were found by Zhao et al. (2017) who used blockiness (defined as '1/*m*') to create virtual particle assemblies in DEM. They also found that a high packing density does not necessarily correspond to high $CN_{ave}$, cubic-like particle packings with high particle orientational alignment may have high packing density but low $CN_{ave}$.

Even though DEM enables the effects of particle shape on $CN_{ave}$ to be studied, the particle shape indicators (aspect ratio) cannot cover the whole range of particle shapes encountered in natural sands as discussed by Fei et al. (2019).

X-ray computed tomography (CT) sheds lights onto the analysis of microstructure (Druckrey et al. 2017; Fei et al. 2019; Nadimi et al.) in irregular natural sands and makes calculating three-dimensional (3D) sphericity and roundness of each grain in the sands possible. The present work selected five sands and rigorously quantified the particle size, 3D sphericity and roundness, CN of each grain in the sand and the $CN_{ave}$ of each sand from CT images. This work aims to bridge the gap between the particle shape, CN of each grain and $CN_{ave}$ in the real sands.

## Materials

As shown in Fig. 1, five natural sands with distinct grain shape but similar diameter ($D_{50}$) were selected. 'Glass beads' are nearly spheres made of silica with silver coats. 'Ottawa sand' (ASTM 2017) particles are more irregular than that of glass beads but still have relatively round corners. Similar to Ottawa sand, grains in 'angular sand' are made of quartz but with sharp corners. 'Crushed schist A' has even more irregular particles which are made of chlorites. Grains in 'crushed schist B' consist of both quartz and biotite, have the most irregular shape and more than half of them are elongated and platy. The $D_{50}$, the particle size range and the sorting index SI (the ratio of standard deviation to the equivalent mean particle size, as defined by Ahmed and Lebedev (2019)) of these sands are summarised in Table 1. A soil with lower SI means that it is well sorted but poorly graded. Please note that these parameters were calculated using four representative element volumes (REVs) whith dimensions of 4.5×4.5×4.5 mm and were chosen from top-left, top-right, bottom-left and bottom-right regions of each sample. The number of particles in a single REV excluding the particles on the border is also shown in Table 1.

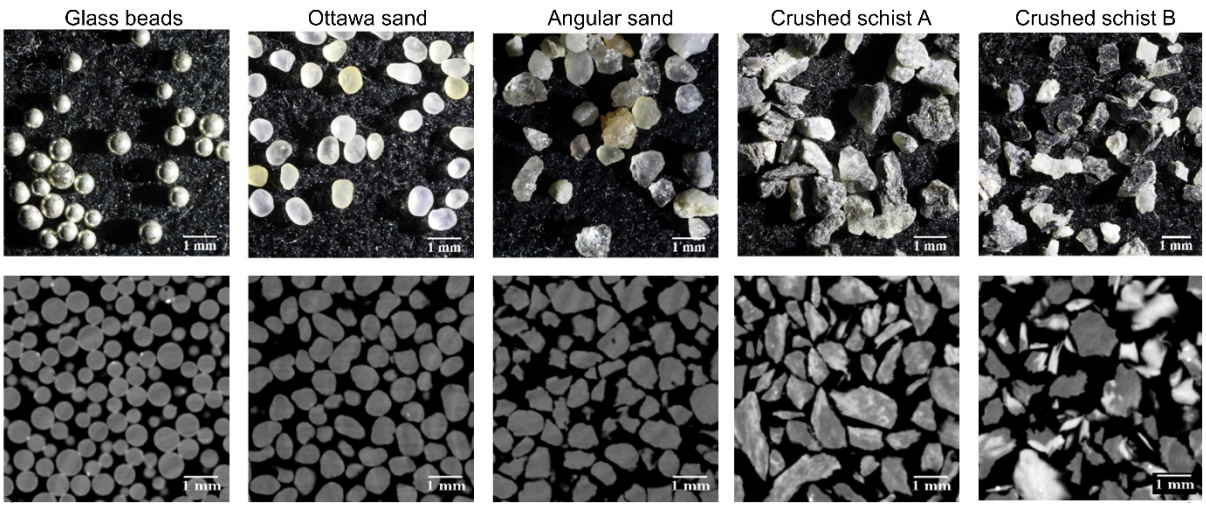


**Fig. 1 Five sands with distinct particle shape. The pictures in the top row were photographed while the images in bottom row were CT scanned with a pixel size of 13 µm.**

**Table 1 Particle size and sorting index (SI) of the studied granular materials**

| Sample | $D_{50}$ (mm) * | $D_{50}$ (mm)^ | Particle size range (mm) * | Particle size range (mm) ^ | *SI* | Number of particles in a REV^ |
|---|---|---|---|---|---|---|
| Glass beads | 0.60 | 0.60 | 0.50 – 0.70 | 0.40 - 0.80 | 0.14 | 270 |
| Ottawa sand | 0.73 | 0.76 | 0.60 – 0.85 | 0.58 - 0.94 | 0.22 | 118 |
| Angular sand | 0.89 | 0.68 | 0.60 – 1.18 | 0.39 – 0.99 | 0.22 | 100 |
| Crushed schist rock A | 0.84 | 0.58 | 0.50 – 1.18 | 0.23 – 0.95 | 0.36 | 119 |
| Crushed schist rock B | 0.84 | 0.61 | 0.50 – 1.18 | 0.16 - 1.10 | 0.28 | 94 |

* Diameter from sieve analysis.
^ Equivalent ball diameter calculated from particle volume after CT reconstruction.

# Methods

The five sands are air-pluviated into relatively small PVC containers and scanned at the Australian Synchrotron to then extract particle shape and CN.

To date, various particle shape descriptors using different definitions have been proposed to characterise particles (Cho et al. 2006; Hryciw et al. 2016; Legland et al. 2016; Sneed and Folk 1958; Wadell 1932). Some two-dimensional (2D) descriptors were compared against 3D (true) descriptors in (Rorato et al. 2019). Upon a critical assessment and comparison of the existing definitions of particle shape descriptors, Fei et al. (2019) suggested that the combination of 3D sphericity (*S* in Equation 2) and roundness (*R* in Equation 3) can capture the shape of most irregular particles reasonably well:

$$S = \frac{36\pi V^2}{SA^3} \tag{2}$$

$$R = \frac{\sum r_i / N}{r_{max-in}} \tag{3}$$

where $V$ is the particle volume, $SA$ is the particle surface area, $r_i$ is the radius of each one out of N corners in a particle and $r_{max-in}$ is the radius of the maximum inscribed sphere of a particle. These variables and the CN of each grain in the packings are obtained following the procedures detailed in (Fei et al. 2019) with some corrections as outlined next.

The isolation of individual grains from CT images is required to calculate their geometrical features. This is a non-trivial task given that grains in natural sands are in contact each other, thus the framework shown in Fig. 2 was proposed to reconstruct individual particles. Particle surface area $SA$ and volume $V$ are required to calculate sphericity $S$ in Equation 2, whereas curvature $1/r_i$ in Equation 3 needs to be computed for roundness $R$. Pixel-counting with the saw-tooth particle surface (Fig. 2(e)) may result in overestimation of particle surface area and volume as well as incorrect roundness. Hence, the framework used here also includes a step to generate a smooth particle surface for more accurate estimations of sphericity and roundness from CT images.

Each sand was air-pluviated into a PVC cylinder ($d$ = 50 mm, $h$ = 120 mm) and scanned at the Australian Synchrotron to achieve sequential CT images with a pixel size of 13 μm (related to image resolution). The selection of sample size and pixel size is a trade-off, noting that images with a small pixel size (i.e., higher image resolution) can be used to identify more accurate interparticle contact area (Persson et al. 2004; Wiebicke et al. 2017) but does not significantly affect CN. CT images (Fig. 2(a)) with a REV of 4.5×4.5×4.5 mm (Fig. 2(b)) were firstly denoised by applying a median filter and a non-local mean filter in Fiji (Schindelin et al. 2012). These filters do not blur the images and keep the particle edge/boundary sharp. Applying the filters may comparatively smooth the particle surface but cause subtle loss of contacts formed by angular edges (Ahmed and Lebedev, 2019). The post-processed results were shown in Fig. 1. Next, the widely used Otsu threshold segmentation (Otsu 1979) was applied to binarize the solid and void phases (Fig. 2(c)). A plugin named MorphoLibJ (Legland et al. 2016) in Fiji (Schindelin et al. 2012) was employed to execute watershed segmentation on solids (Fig. 2(d)) and obtain individual voxelated particles (Fig. 2(e)). Six-voxel neighbourhood was selected in the watershed

segmentation to reduce the overestimation of particle surface area and volume (Fonseca et al. 2012). At last, the saw-tooth surface of the voxelated particles was smoothed by using the Taubin smoothing method (Taubin 1995). Taubin smoothing method includes two parameters $\lambda$ and $\mu$ to control shrinkage and inflation, respectively. Here $\lambda$ = 0.6 and $\mu$ = -0.3 were determined after calibrating the particle surface area and volume of CT reconstructed sphere and ellipsoid against theoretical values, following (Fei et al. 2019).

An in-house program (Fei et al. 2019) was used to identify the interparticle contact by searching the shared boundary voxels between particles. The number of interparticle contacts was then used to calculate the CN of each grain and the $CN_{ave}$ of each sample of the sands.

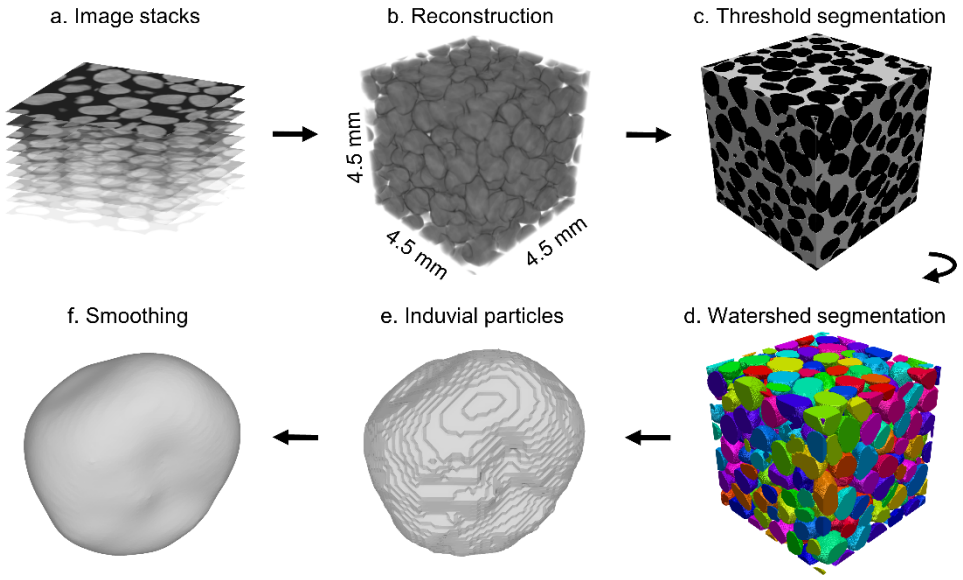


**Fig. 2 Procedures to achieve individual particles of Ottawa sand from CT images**

## RESULTS AND DISCUSSION

For each sand, four subsamples from top-left, top-right, bottom-left and bottom-right regions of each sample were selected to calculate the CN and particle shape characteristics of every sand grain. The distributions of CN for the four subsamples from each material are shown in Fig. 3. It is clear from the fitted normal distribution curves that the $CN_{ave}$ in the round glass beads is about 7. As glass bead size is not uniform, the maximum CN of a glass bead is 13 (slightly higher than in mono-dispersed Face Centred Cubic (FCC) sphere packings, which may indicate a slight overestimation of $CN_{ave}$). The $CN_{ave}$

then decreases to 5.3 and 5.7 in crushed schist A and B. The maximum CN in the very irregular crushed schist B is above 14 which is possible even for ellipsoids having strong friction (Donev et al. 2004). Besides particle shape, gradation also varies in all five sands according to the SI shown in Table 1. Hence, well-graded but more irregular particle packings may have lower $CN_{ave}$ in real sands in contrast with the findings that better gradation can increase the $CN_{ave}$ in sphere packings (Minh and Cheng 2013). Fig. 3 shows that an irregular particle (e.g., crushed schist) may have higher CN than a round particle (e.g., Ottawa sand), this is true when one focuses on single grains. The effect of particle shape on average value of coordination number of a grain packing may be different from its effect on the coordination number of a single grain.

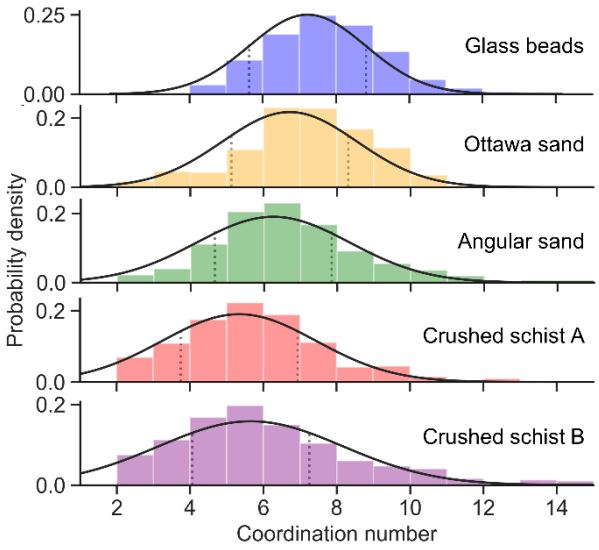


**Fig. 3 Distribution of coordination number and fitted normal distribution curve. The coordination number at the crest of the normal distribution curve is $CN_{ave}$. The vertical dotted lines show the limits of two standard deviations around $CN_{ave}$.**

To further quantify the impact of particle shape on coordination number, Fig. 4 shows the computed 3D sphericity and roundness of each grain in the five sands and their probability distributions. Note that DEM studies typically use aspect ratio, a more straightforward parameter for ellipsoids than sphericity and roundness. Both sphericity and roundness range between 0 and 1. It is noticeable that the glass beads are not perfect spheres and the bright spots in the CT images of glass beads (Fig. 1) resulting from their silver coats could lead to the defects in reconstructed surface mesh, artificial low roundness

in some particles and larger $CN_{ave}$ in the sample. The average sphericity and roundness decrease from round glass beads to irregular crushed schist B, which indicates that these descriptors capture well their particle shape. Excluding the glass beads, sphericity shows a larger range than roundness and the range of sphericity expands gradually from glass beads to crushed schist B.

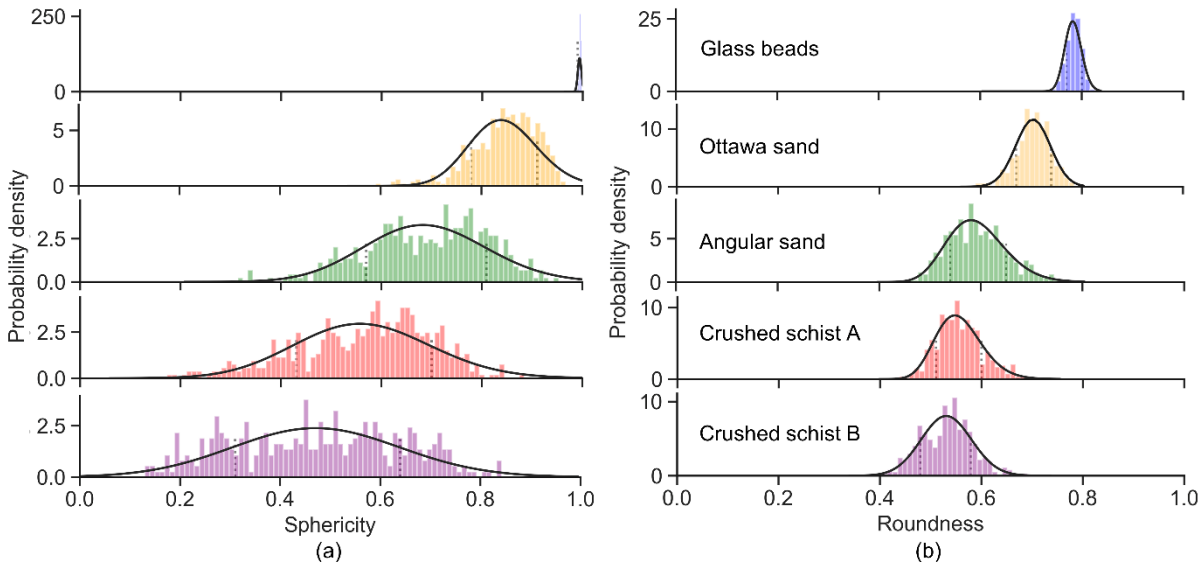


**Fig. 4 Distribution of sphericity (a) and roundness (b) with fitted normal distribution curves. The vertical dot lines show the limits of two standard deviations around the average.**

Since DEM studies set the ellipsoids having the same equivalent diameter, we also computed the equivalent diameter from the particle volume *V* in Equation 2. For a clearer visualisation, particles from only one of four REVs of each specimen were used to show the relationship between equivalent diameter, the average of 3D sphericity and roundness, and CN of each grain in Fig. 5. The averaging of sphericity and roundness was proposed by Cho et al. (2006) based on the commonly used particle shape chart (Krumbein and Sloss 1963), and selected here since sphericity and roundness show similar trends to each other in Fig. 4. The red data points at the right of Fig. 5(a) shows larger CN because the grains have a larger equivalent diameter (Fonseca et al. 2014). This trend can also be clearly observed in each material from Fig. 5(b) – (f). Within a certain soil such as angular sand (Fig. 5(d)), the increasing trend is not only observed from left to right but also from top to bottom. This trend indicates that a more irregular large grain may exhibit higher CN in a given sand. For a given equivalent diameter, a subtle

increase in the CN of more irregular grains can also be seen along the dashed line in each sand, which is the same as the trend reported in DEM based papers (Delaney and Cleary 2010; Donev et al. 2004; Gan et al. 2017; Zhou et al. 2011) but different from the decreasing trend of $CN_{ave}$ in more irregular sand packings as shown in Fig. 3.

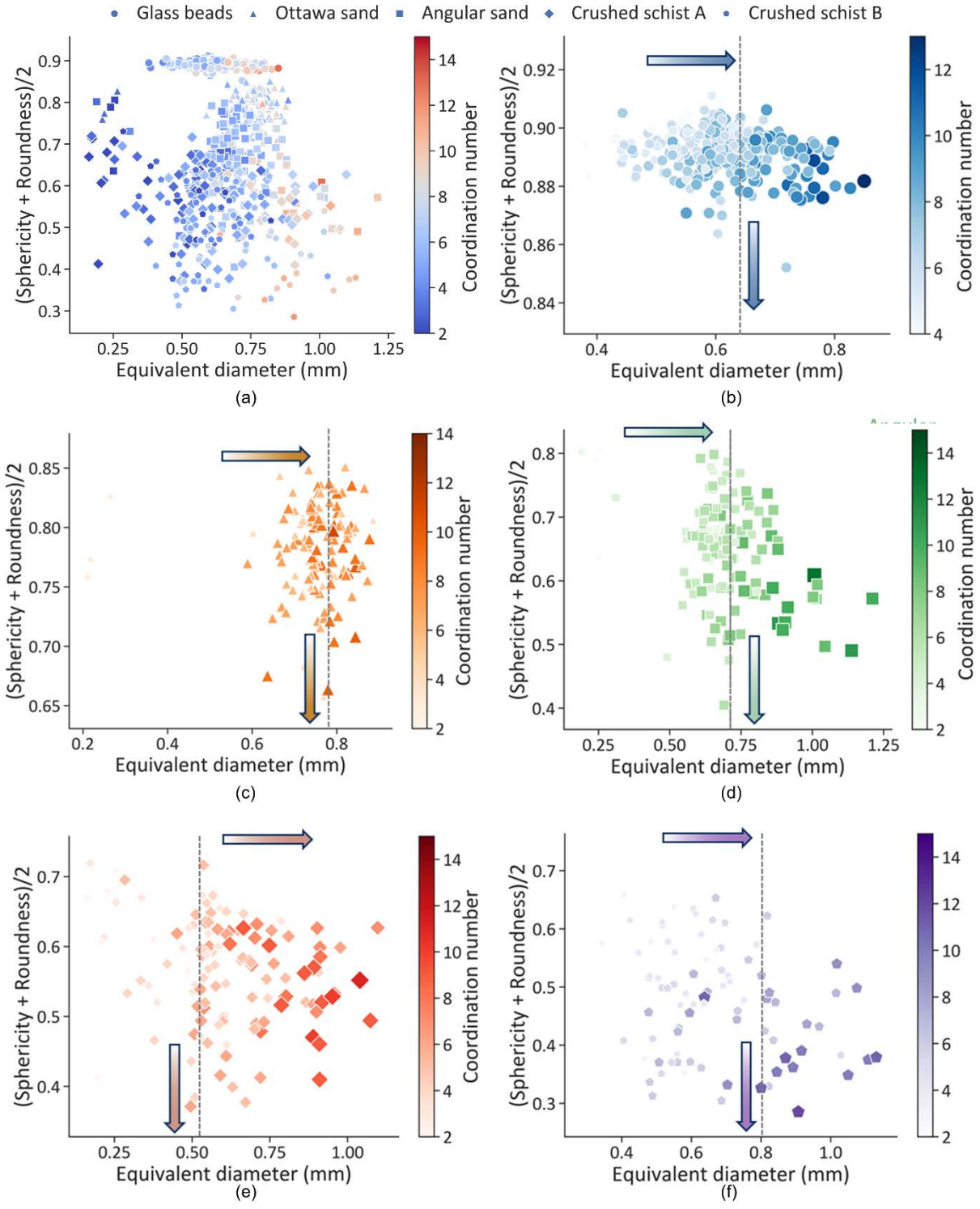

**Fig. 5 A subsample from each material are selected. For each grain, its particle shape is plotted against equivalent diameter and rendered by coordination number. Grains from (a) combined five sands, (b) glass beads, (c) Ottawa sand, (d) angular sand, (e) crushed schist A, (f) crushed schist B.**

A qualitative explanation for these observations can be rooted in the micro-structural arrangement of particles in a packing and the inherent (reasonable) assumptions used in DEM modelling. CN is known to be related to the particle rolling and sliding when packing particles together under gravity (Delaney and Cleary 2010; Donev et al. 2004). DEM studies show that ellipsoid packings have higher $CN_{ave}$ than that in sphere packings because an ellipsoid has more rotational degrees of freedom to be restricted than a sphere in sphere packings (Delaney and Cleary 2010; Donev et al. 2004; Gan et al. 2017; Zhou et al. 2011) as shown in Fig. 6 (a) and (b). Let us illustrate this by focusing on the degree of freedom on the two-dimensional planes in Fig. 6 (a) and (b): the central 'spherical' particle cannot move when it is in contact with other three spherical particles. In contrast, an 'ellipsoidal' particle restricted by three other ellipsoids can still rotate and have more neighbours to contact, resulting in a higher CN for itself. 3D CT reconstructed geometry of each sand is also visualised in Fig. 6 (c) – (g) to compare the particle arrangement. In the angular sand (Fig. 6 (e)), particle No.0 is jammed by only two particles. In the more irregular crushed schist B (Fig. 6 (g)), the platy particle No. 0 can be supported stably by a single particle No. 1. Hence, the orientational alignment of the irregular particles results in a low $CN_{ave}$ even though the single irregular particle has the possibility of high individual CN. Additionally, the concave surface on irregular particles may induce interlocking so that a particle cannot move even when touching fewer particles (Fig. 6 (f)). In addition, the irregular particle may also exhibit higher roughness (another particle shape descriptor at a smaller scale than sphericity and roundness). Higher roughness is related to a higher coefficient of friction which resists the rotation and sliding of particles during gravity deposition and shear loading. However, DEM simulations usually set sliding and rolling friction coefficient the same for all the particles in the assembly and also generally assumes that particles with different particle shape have the same Young's modulus (which may be different in reality). Furthermore, the detection of CN in DEM is sensitive in the selection of a critical separation

distance (Zhou et al. 2011) which is also assumed as the same for all the particles. These limitations may be the cause of the contrasting observations made in this paper.

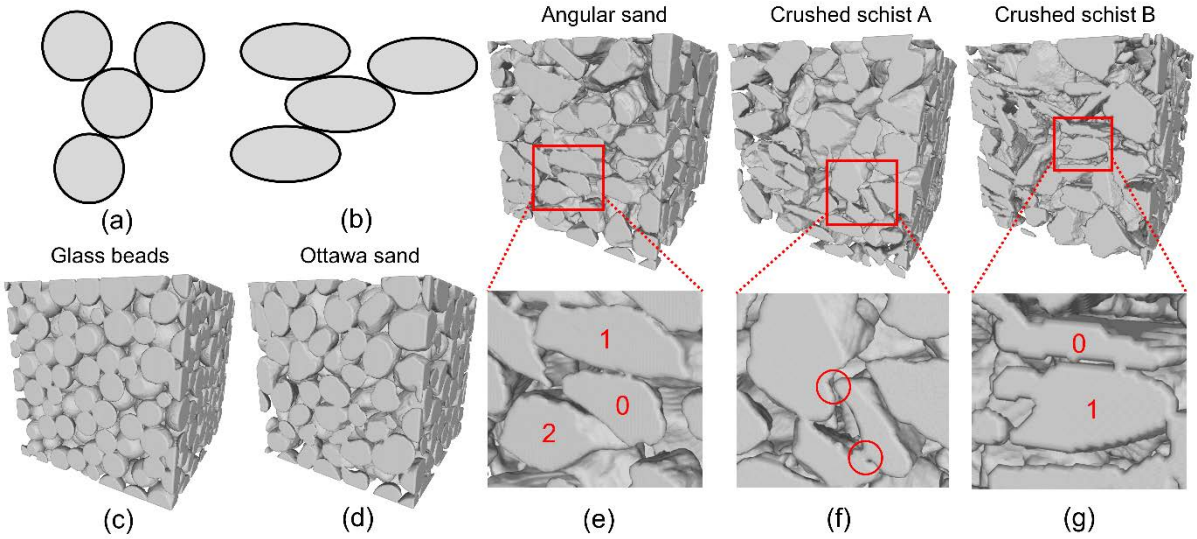


**Fig. 6 Schematic sphere packings (a) and ellipsoid assembly (b), and CT reconstructed glass beads (c), Ottawa sand (d), angular sand (e), crushed schist A (f) and crushed schist B (g).**

## CONCLUSIONS

This study investigates the impact of particle shape on coordination number in real sands with the help of computed tomography (CT) and image processing techniques. In a given sand, a more irregular grain has subtle higher *individual* coordination number (CN) and the CN of the grain increases with increasing particle size. However, the trend may be different when comparing the *average* coordination number ($CN_{ave}$) in different sands. An air-pluviated more irregular particle packing with poor gradation may result in lower $CN_{ave}$ due to particle orientational alignment, particle interlocking and surface roughness.

The trend of the $CN_{ave}$ in this paper is different from that reported from DEM studies since this work is based on real sands and uses different particle shape descriptors. The reasons of this apparent discrepancy are a key finding in this work. It is hard to ensure that the different sands have the same average equivalent diameter as well as gradation compared with the flexible setting in DEM. However, DEM studies include simplifications such as setting a certain critical separation distance to detect all

particle contacts and usually assume that particles with different particle shape have the same Young's modulus, sliding and rolling friction coefficients (they may be different in reality); all of which may impact on the characterization of actual soils at the microscale, even in the absence of external load but when using DEM to generate samples by gravity deposition.

The particle surface roughness and interlocking have not been quantified in this article and are interesting topics for future research.

## DATA AVAILABILITY

Some or all data, models, or code that support the findings of this study are available from the corresponding author upon request.

## ACKNOWLEDGEMENTS

The Imaging and Medical Beam Line (IMBL) at the Australian Synchrotron, Dr A Maksimenko and other beam scientists are acknowledged for their support. The first author thanks The University of Melbourne for offering the Melbourne Research Scholarship.

## REFERENCES

Ahmed, Z., and Lebedev, M. (2019). "Elastic properties of sands, Part 1: Micro computed tomography image analysis of grain shapes and their relationship with microstructure." *Geophysical Prospecting*, 67(4), 723-744.

ASTM (2017). "C778-17 standard specification for standard sand." *ASTM International, West Conshohocken, PA*.

Cho, G., Dodds, J., and Santamarina, J. (2006). "Particle Shape Effects on Packing Density." *Stiffness and Strength of Natural and Crushed Sands-Internal Report, Georgia Institute of Technology, 33pp*.

Delaney, G. W., and Cleary, P. W. (2010). "The packing properties of superellipsoids." *EPL (Europhysics Letters)*, 89(3), 34002.

Donev, A., Cisse, I., Sachs, D., Variano, E. A., Stillinger, F. H., Connelly, R., Torquato, S., and Chaikin, P. M. (2004). "Improving the density of jammed disordered packings using ellipsoids." *Science*, 303(5660), 990-993.

Druckrey, A., Alshibli, K., and Al-Raoush, R. (2017). "Discrete particle translation gradient concept to expose strain localisation in sheared granular materials using 3D experimental kinematic measurements." *Géotechnique*, 68(2), 162-170.

Fei, W., Narsilio, G. A., and Disfani, M. M. (2019). "Impact of three-dimensional sphericity and roundness on heat transfer in granular materials." *Powder Technology*, 355, 770-781.

Fei, W., Narsilio, G. A., van der Linden, J. H., and Disfani, M. M. (2019). "Quantifying the impact of rigid interparticle structures on heat transfer in granular materials using networks." *International Journal of Heat and Mass Transfer*, 143, 118514.

Fonseca, J., O'Sullivan, C., Coop, M. R., and Lee, P. (2013). "Quantifying the evolution of soil fabric during shearing using directional parameters." *Géotechnique*, 63(6), 487-499.
Fonseca, J., O'Sullivan, C., Coop, M. R., and Lee, P. (2012). "Non-invasive characterization of particle morphology of natural sands." *Soils and Foundations*, 52(4), 712-722.
Fonseca, J., Sim, W., Shire, T., and O'sullivan, C. (2014). "Microstructural analysis of sands with varying degrees of internal stability." *Géotechnique*, 64(5), 405-411.
Gan, J., Zhou, Z., and Yu, A. (2017). "Effect of particle shape and size on effective thermal conductivity of packed beds." *Powder Technology*, 311, 157-166.
Hryciw, R. D., Zheng, J., and Shetler, K. (2016). "Particle roundness and sphericity from images of assemblies by chart estimates and computer methods." *Journal of Geotechnical and Geoenvironmental Engineering*, 142(9), 04016038.
Krumbein, W. C., and Sloss, L. L. (1963). "Stratigraphy and sedimentation."
Legland, D., Arganda-Carreras, I., and Andrey, P. (2016). "MorphoLibJ: integrated library and plugins for mathematical morphology with ImageJ." *Bioinformatics*, 32(22), 3532-3534.
Minh, N., and Cheng, Y. (2013). "A DEM investigation of the effect of particle-size distribution on one-dimensional compression." *Géotechnique*, 63(1), 44.
Nadimi, S., Fonseca, J., Andò, E., and Viggiani, G. (2019). "A micro finite-element model for soil behaviour: experimental evaluation for sand under triaxial compression." *Géotechnique*, 0(0), 1-6.
Otsu, N. (1979). "A threshold selection method from gray-level histograms." *IEEE transactions on systems, man, and cybernetics*, 9(1), 62-66.
Persson, B., Albohr, O., Tartaglino, U., Volokitin, A., and Tosatti, E. (2004). "On the nature of surface roughness with application to contact mechanics, sealing, rubber friction and adhesion." *Journal of physics: Condensed matter*, 17(1), R1.
Rorato, R., Arroyo, M., Andò, E., and Gens, A. (2019). "Sphericity measures of sand grains." *Engineering Geology*, 254, 43-53.
Schindelin, J., Arganda-Carreras, I., Frise, E., Kaynig, V., Longair, M., Pietzsch, T., Preibisch, S., Rueden, C., Saalfeld, S., and Schmid, B. (2012). "Fiji: an open-source platform for biological-image analysis." *Nature methods*, 9(7), 676.
Shire, T., and O'Sullivan, C. (2013). "Micromechanical assessment of an internal stability criterion." *Acta Geotechnica*, 8(1), 81-90.
Sneed, E. D., and Folk, R. L. (1958). "Pebbles in the lower Colorado River, Texas a study in particle morphogenesis." *The Journal of Geology*, 66(2), 114-150.
Taubin, G. "Curve and surface smoothing without shrinkage." *Proc., Computer Vision, 1995. Proceedings., Fifth International Conference on*, IEEE, 852-857.
Wadell, H. (1932). "Volume, shape, and roundness of rock particles." *The Journal of Geology*, 40(5), 443-451.
Wang, J., Wu, S., Zhao, L., Wang, W., Wei, J., and Sun, J. (2019). "An effective method for shear-wave velocity prediction in sandstones." *Marine Geophysical Research*, 40(4), 655-664.
Wiebicke, M., Andò, E., Herle, I., and Viggiani, G. (2017). "On the metrology of interparticle contacts in sand from x-ray tomography images." *Measurement Science and Technology*, 28(12), 124007.
Zhao, S., Zhang, N., Zhou, X., and Zhang, L. (2017). "Particle shape effects on fabric of granular random packing." *Powder technology*, 310, 175-186.
Zhou, Z.-Y., Zou, R.-P., Pinson, D., and Yu, A.-B. (2011). "Dynamic simulation of the packing of ellipsoidal particles." *Industrial & Engineering Chemistry Research*, 50(16), 9787-9798.